LA-UR -81-1566

TITLE: INFLUENCES ON TARGET IRRADIATION SYMMETRY IN CO_2 LASER-FUSION EXPERIMENTS

AUTHOR(S): Robert L. Carman

MASTER

SUBMITTED TO: Proceedings of Topical Conference on Symmetry Aspects of Inertial Fusion Implosions
Naval Research Laboratory
Washington, DC

University of California

LOS ALAMOS SCIENTIFIC LABORATORY
Post Office Box 1663 Los Alamos, New Mexico 87545
An Affirmative Action/Equal Opportunity Employer

DISTRIBUTION OF THIS DOCUMENT IS UNLIMITED

Form No. 836 R3
St. No. 2629
12/78

UNITED STATES
DEPARTMENT OF ENERGY
CONTRACT W-7405-ENG. 36

INFLUENCES ON TARGET IRRADIATION SYMMETRY IN CO_2 LASER-FUSION EXPERIMENTS

Robert L. Carman

University of California
Los Alamos National Laboratory
Los Alamos, NM 87545

Lasers are a source of focusable, but limited energy. As such, the achievement of thermonuclear burn in laser pellets requires compression of the fuel to ~ 10^4 times normal density, while simultaneously heating the fuel to several keV temperatures. Many coronal effects can substantially influence the ability of the laser light to achieve these conditions in a pellet, where the radius of the compressed region is at least one TN α-particle mean-free path. In simple targets, the laser energy must be deposited uniformly while preheat from high energy particles and x-rays must be minimized. Use of a CO_2 laser implies that the radiation pressure exerted by the light is very high, leading to a substantial modification of the plasma density profile over those associated with free hydrodynamic expansion.[1,2] The resulting steep density gradients preclude efficient laser deposition by the inverse-bremsstrahlung process.[3] Instead, resonance absorption becomes the dominant mechanism for energy deposition. Under these conditions, PIC computer simulations have revealed the presence of very large amplitude and highly nonsinusoidal surface plasma waves, which are found

to eject hot electrons from the plasma.[1] These plasma waves are also responsible for the efficient production of visible and uv harmonics of the CO_2 laser.[1] Because of this intimate connection between resonance absorption, hot electron generation, and high harmonic production, we will find it useful to use the harmonic response of the plasma as a means for studying the uniformity of energy deposition as well as for studying hot electron generation in CO_2 laser-produced plasmas.

In 1977, the efficiency for producing harmonics of the incident irradiation during laser fusion experiments was studied, both at the Naval Research Laboratory[4] and at the National Research Council[5] using Nd:glass and CO_2 lasers, respectively. In Fig. 1, we show a compilation of this data which was purposely taken at the same value of the parameter $I\lambda^2 = 10^{16}$ W $\mu m^2/cm^2$. Note the similarity in behavior, as well as the ~ 6-fold drop in backscattered harmonic light with each increase in the order of the harmonic generated by both lasers. Also, these results conformed with what is expected for the nonlinear optical response from studies of condensed media.

A very different nonlinear response was observed in CO_2 laser produced plasmas when the incident intensity was increased. The two spectra of Fig. 2, taken from Ref. 1, demonstrate the new result. Harmonics from the 16th order through the 29th order were observed at the Helios laser facility, while the 16th order through the 20th order were observed at the Gemini laser facility. When the results of a radiometric calibration are used to correct the amplitudes, we find that the relative peak conversion efficiencies are the same to within a factor of 2 across

the entire spectrum in both cases. Furthermore, neither of these spectra were obtained in the backward direction. Instead, the Gemini spectrum was obtained with the direction of observation of the spectrograph being in the horizontal plane of the incident laser focusing parabola and 105° around from the laser optic axis. The Helios spectrum was obtained with the direction of observation being in the plane of one of the axes of the laser focusing parabolas and ~ 30° around from this laser beam optic axis. Since these data were taken, several other observation directions have been employed with no substantial variation in efficiency being noted. However, there were enough variables to preclude any quantitative comparison to construct an angular distribution.

Numerical simulations[1] were carried out by D. Forslund and J. Kindel, which showed that under equilibrium conditions, the number of harmonics produced was related to the density N_{upper} of the upper shelf for conditions where profile modification was important. In fact, N_{upper} was found to be approximately the critical density for the highest harmonic efficiently produced, or

$$N_{upper} \sim n^2 N_{crit} \ (CO_2). \qquad (1)$$

This relationship is reasonable, since it implies that under conditions of a very steep density profile, all of the harmonics up to nω have the same spatial turning point while (n + 1)ω has a much larger skin depth, and thus does not turn in this same spatial location. Furthermore, all of the first n harmonics only experience the plasma

density of the lower shelf until they turn, while $N_{lower} \sim 0.1\ N_{crit}$ (CO_2) from the same simulations,[1] implying that very little dispersion exists in this region of space. Thus, Eq. (1) is analogous to the usual concept of phase matching.

Additional Gemini data indicates that at an incident laser intensity of $I = 2.3 \times 10^{15}$ W/cm^2 up to 42 harmonics are produced at high efficiency.[6] This data implies that N_{upper} is as high as 1-2 x 10^{22} e/cm^3. If we assume that profile modification, associated with radiation pressure balancing hydrodynamic expansion, dictates the value of N_{upper}, we can develop a model which predicts the number of harmonics n versus plasma parameters. First, the balance condition is given by

$$(2-\alpha)\ \frac{I}{c} = N_{upper}\ T_e\ , \qquad (2)$$

where α is the laser absorption fraction, the effects of isotropic scattering and refraction of laser light are ignored, and hydrodynamic expansion is assumed to proceed according to the ideal gas law. T_e is the background plasma temperature assumed to be in LTE. Combining Eqs. (1) and (2) with the definition of N_{crit} (CO_2) yields

$$n = \frac{e}{c}\left[\left(\frac{2-\alpha}{\pi c}\right)\ \frac{I\lambda^2}{T_e}\right]^{1/2}\ . \qquad (3)$$

Assuming $\alpha = 30\%$, $\lambda = 10.6\ \mu m$ and $I = 2.3 \times 10^{15}$ W/cm^2, 42 harmonics implies that $T_e = 46$ eV. This temperature is about 10 times lower than usually inferred from x-ray data or calculated by numerical simulations.

We, therefore, conclude that either the local laser intensity is higher than the spatially averaged laser intensity, possibly because of self-focusing, or that the upper shelf density is not correctly predicted by the balance condition of Eq. (2). The experimental situation actually lends some support to both arguments, as we shall see below.

Evidence for Self-Focusing and Laser Filamentation

Over the last year, self-focusing and laser filamentation has been reported by the Naval Researach Lab using a Nd:glass laser,[7] while self-focusing was reported by the National Research Council using a CO_2 laser.[8] While both of these experiments were carried out under conditions where the plasma scale heights were much larger than would be expected under our experimental conditions, we can use a simple phenomenological model of self-focusing to scale from these results to our conditions, in an attempt to appraise if self-focusing should be expected. Also, we can more closely examine our data to look for some experimental evidence.

This model was first used by P. Kelley[9] and employs the concept of a critical power for self-focusing. In one beam diffraction length or Rayleigh range z_D, the beam will double in size, where

$$z_D = d^2/1.22\lambda. \tag{4}$$

On the other hand, in a self-focusing distance z_{SF}, the beam will collapse to a dimension of the order of one wavelength, where

$$z_{SF} = d\sqrt{\frac{n_0}{\Delta n}} \quad . \tag{5}$$

$\Delta n = n - n_o = n_2 \quad E^2 = \frac{32\pi\, n_2 \bar{I}}{c}$, is the maximum refractive index change, $\bar{I}$ is the spatially averaged incident laser intensity estimated as 25% of I_{peak}, $n_o = (1 - \omega_p^2/\omega^2)^{1/2}$, and ω_p is the electron plasma frequency. For the case of a spatially structured beam, the diameter d becomes the scale of the spatial structure in both Eqs. (4) and (5). By equating these two expressions, we arrive at the condition which defines which effect dominates, namely the condition for diffractionless propagation in terms of a critical power,

$$P_{crit} = (1.22\,\lambda)^2 \frac{n_o\, c}{128\, n_2}. \tag{6}$$

From the previous CO_2 laser self-focusing experiment,[8] we can estimate $P_{crit} = 10^8$ W. If we further assert that the nonlinear coefficient n_2 is not implicitly wavelength-dependent, then $P_{crit} = 10^6$ W should apply for the Nd:glass laser results.[7] These estimates are consistent with both results as reported. If we now combine Eq. (5) and (6), we arrive at a scaling law for Z_{SF} in terms of P_{crit} assuming similar plasma conditions, namely

$$Z_{SF} = \frac{d}{1.22\,\lambda} \sqrt{\frac{4\, P_{crit}}{\pi\, \bar{I}}}. \tag{7}$$

In our experiments, the laser beams are focused with f/2.4 optics, which, for a diffraction-limited beam implies d ≈ 62 μm. Because our measured half-energy diameter for the focused beams is d ≈ 85 μm, we need not be concerned about which d we choose for our estimates. Table I lists Z_{SF} for two different values of d, namely 50 μm and 100 μm, as a function of incident intensity I. Because our laser pulses rise in ~ 200 ps to their peak intensity, while an expansion velocity $v_{exp} \sim 2 \times 10^7$ cm/s is reasonable, we would expect our plasma scale height to be ~ 40 μm. Therefore, we should expect self-focusing to be important for I ~ 10^{15} W/cm^2. We noted, in the Gemini experiment, that the number of harmonics produced for 2-3 x 10^{14} < I < 10^{15} W/cm^2 was typically twice as few as for I > 10^{15} W/cm^2. This tends to support the estimate above for when self-focusing may be occurring while indicating that the intensity in the self-focused region was approximately four times enhanced over the spatially-averaged intensity.

In this same series of Gemini experiments, more direct evidence for something happening at I > 10^{15} W/cm^2 was obtained by the x-ray pinhole cameras. These cameras were located directly above the laser axis at an angle of ~ 45°. The targets were carbon wires of 250-μm-diam, and their axes were oriented vertically. The pinhole camera was filtered to transmit principally 1-2 keV x-rays. The pinhole actually was a doublet consisting of a 25 μm and a 50 μm hole separated by 1 mm. The resulting photographs are shown in Fig. 3, with incident laser intensity as a parameter. For I ≈ 1-2 x 10^{14} W/cm^2, we observe a smooth emission region of < 150-μm-diam. For the same filtration and I ≈ 1.4 x 10^{15} W/cm^2, the emission region is approximately the same size, but

highly structured. Actually, the structure is unresolved, being limited by the 25-μm-diam of the smallest pinhole. However, further increases in intensity cast some doubt on the uniqueness of this interpretation, since the x-ray emission region is seen to expand in size and elongate in the direction of the axis of the carbon wires, suggesting that surface currents combined with possible current pinching might explain the small size of the x-ray emitting regions. Possibly, the truth is that both effects are contributing.

In earlier work carried out at Gemini,[10] it was noted that the angular distribution of electrons switched from being fairly smooth to one with much angular structure for $I > 10^{15}$ W/cm^2. Similar results have been obtained more recently when the angular distribution of fast ions was investigated at Gemini[11]. However, due to the sensitivity of ions to local magnetic fields, these ion results have less possible bearing than the electron results. Also, while these observations could be explained by the presence of self-focusing, they too are not a verification.

Recent results obtained at the Helios laser facility, where higher laser intensities are available, provide more indirect evidence for both self-focusing as well as laser filamentation. In Fig. 4, we show a high resolution spectrum of the 16th harmonic light produced by irradiating a hollow nickel sphere of 250-μm-diam with $I \sim 1.5 \times 10^{16}$ W/cm^2. Similar spectra have been obtained for the 16th through the 20th harmonics. These spectra were obtained using a 1.0-m McPherson spectrograph equipped with a 1200-line/mm grating blazed for 500 nm. The

demonstrated spectral resolution was < 0.75 cm^{-1}. The relay lens system was purposely defocused so as to spatially average the harmonic light at the entrance slit, thus removing much of the alignment difficulties. Note that two different frequency modulations are present. The high-frequency modulation is very uniform and has a spacing of 1.8 ± 0.05 cm^{-1} across the entire spectrum. The low-frequency modulation is less uniform and has an average spacing of ~ 9 cm^{-1}. Finally, the center of the spectrum is located at the expected 16th harmonic of the P(20) transition in the 10 μm band of the CO_2 laser to an accuracy of ~ 1 cm^{-1}.

While this spectrum could be explained by Doppler shifts from a moving mirror corresponding to a motion of the plasma critical surface, an average velocity of nearly 10^9 cm/s would be required. The motion would have to be an undulation rather than a smooth translation in order to induce two separate modulations. Therefore, even for times of the order of 100 ps, the critical surface would have to travel several target diameters under these conditions. Furthermore, because no net center frequency shift is observed, the critical surface must move symmetrically outward and then inward, or vice versa in exactly the same way. These requirements seem implausible. On the other hand, the spectrum can be readily explained, if self-focusing and self-phase modulation had occurred.[12] The Helios oscillator is known to operate typically on three or four rotational lines in the 10 μm band simultaneously, namely P(16), P(18), P(20), and P(22). More than half of the output energy is obtained in the P(20) transition. The average spacing of these transitions is 1.79 cm^{-1}.

while the pressure broadened linewidth of each transition is ~ 0.3 cm^{-1}. We believe that the ~ 150 separate lines seen in Fig. 4 are due to frequency sideband generation,[13] where

$$\omega_1 + \omega_2 = \omega_3 + \omega_4. \tag{8}$$

In this process ω_1 and ω_2 could be any pair of laser output lines while, in general, ω_3 and/or ω_4 would be new frequencies. By choosing all possible combinations of initial frequencies we can increase the number to 3q-2 final frequencies. If we now repeat this process two to three more times, again taking all possible pairings, we can easily arrive at the required number of lines. Now in order to have this infrared spectrum produce a 16th harmonic spectrum containing the observed high-frequency modulation, we perform a sum frequency mixing where the various combinations of 16 lines are used.

The importance of this interpretation of the high-frequency modulation in Fig. 4 is that it provides for a strong argument for the presence of self-focusing. Frequency sideband generation is identical to nondegenerate four-wave mixing (NDFWM). However, in a nonlinear medium which displays little dispersion in the nonlinearity, the presence of NDFWM implies the existence of degenerate four-wave mixing (DFWM) or, in other words, the same process indicated by Eq. (8) but where all the frequencies are the same.[14] To understand this, we first must recognize that a similar momentum equation must also be satisfied along with Eq. (8), namely

$$\vec{k}_1 + \vec{k}_2 = \vec{k}_3 + \vec{k}_4. \tag{9}$$

In the DFWM process, the four frequencies are identical, but the k-vectors are noncollinear. In other words, we are talking about spatial sideband generation. In earlier work,[14] it was shown that this scattering process is the fundamental scattering process associated with self-focusing. Thus, the presence of NDFWM suggests that DFWM is occurring on the P(20) light. The fact that multiple iterations of NDFWM is required to explain the large number of frequency sidebands further suggests that multiple iterations of DFWM has occurred, which implies that the beam has self-focused.[14]

There is a further consequence to the existence of self-focusing. If we recall that the uniphase contours are normal to the light trajectories, we can view self-focusing as a change in the phase of the light which is caused by the nonlinear interaction. Recalling that the phase of a light wave is given by

$$\phi = \vec{k}.\vec{r} - \omega_0 t, \tag{10}$$

where $k = n\,\omega_0\,k.r/c$ and $n = n_0 + 8\pi n_2 I/c$, we see that the spatial change in the phase is introduced because $I_{peak} = I_{peak}(r)$. However, $I = I(t)$ while the center frequency ω of the pulse is defined as

$$\omega = -\frac{\partial\phi}{\partial t} = \omega_0 - \frac{\omega_0\, k.r}{c}\,\frac{\partial n}{\partial t}\,. \tag{11}$$

The last term in Eq. (11) is what is responsible for the effect called self-phase modulation, and it should occur simultaneously with self-focusing unless the path through the nonlinear medium is too short. Usually, self-phase modulation occurs in the region where the laser light is fully focused,

the region usually referred to as the laser filament.[12] According to the theory for self-phase modulation,[15] the average frequency separation in the modulated spectrum, typified by those of Fig. 5,[12] corresponds to the inverse duration of the light contained in the filament. Applying this interpretation to the slowly-varying modulation observed in Fig. 4, we conclude that the light is trapped in the filament for ~ 1.6 ps. Since the filament exists in the subcritical density plasma, where PIC simulations[1] predict the density $N = 0.1\ N_{crit}$, we can convert the trapping time to a spatial extent for the filament. If the light in the filament is a traveling wave, the above duration corresponds to a filament of 500 μm length. On the other hand, the light must be reflected from the critical surface, thus allowing for the possibility that the light trapped in the filament is really a standing wave. This would reduce the length of the filament to 250 μm, or the same spatial extend observed by NRL[7]. Since the length of the filament is dependent principally on linear and nonlinear intensity changes, it would not be too surprising if this length was the same at both 1 μm and 10 μm under the reported conditions. The plausibility that the light is a standing wave is further improved when it is realized that the same nonlinearity responsible for self-focusing, laser filamentation and self-phase modulation can also be responsible for another effect called phase conjugation,[16] where an incident beam of light can be caused to exactly reverse its direction despite the fact that the plasma critical surface is not normal to the average incident k-vector for the light wave.

While it is clear that more direct methods for verifying the existence of self-focusing, self-phase modulation, and laser filamentation must be employed, there is a growing body of indirect evidence or effects easily explained by these laser-light nonlinearities. We shall have more to say about this in the conclusion section.

Transient Plasma Density Effects

While the above discussion on laser self-action seems to explain several observations, there does appear to be an alternative explanation for the harmonic data taken on the Gemini laser facility. While the validity of Eq. (1) seems essential, it is not necessary to require that N_{upper} be self-consistently determined by the balance condition of Eq. (2). An ultrafast Imacon 675 visible streak camera has been used on recent Gemini experiments to examine the temporal aspects of the high harmonic emission.[17] The data clearly shows that the visible harmonic light has a duration of < 200 ps and that this light is emitted during the rising portion of the CO_2 laser pulse. Figure 6 shows a plot of plausible density contours for the same peak intensity if only the laser risetime were changed. We note that in the limit of very fast risetimes τ_1, insufficient hydrodynamic expansion has taken place so that plasma at solid density is fully accessible to the CO_2 radiation. Here ℓ is the skin depth for the laser light. In the opposite limit of very slow risetimes τ_3, we note that the balance between radiation pressure and hydrodynamic expansion pressure has caused the usual profile modification, where the plasma density a distance ℓ inside the density jump is essentially the same as N_{upper} at the density jump. In this limit, we

should expect Eq. (2) to apply. Finally, under the circumstances represented by τ_2, substantially higher densities than N_{upper} are accessible within one skin depth of the density jump.

If this transient model for describing the effective N_{upper} is correct, there should be a substantial change in the number of observed visible and uv harmonics when the laser risetime is changed. Figure 7 shows a series of retraced oscillograms taken using the 5.0 Gigahertz Los Alamos Model 76 oscilloscope, and a Moletron model P-500 pyroelectric detector[18] which looked at a beamsplit portion of the incident laser light. It was found that lower laser intensity, double pulses or long laser risetimes resulted in less than 16 harmonics efficiently produced. On the other hand, high peak intensities and short risetimes produced copious qualities
of harmonic light across the entire visible portion of the spectrum. In the two cases where the peak incident intensity was $I \sim 2 \times 10^{15}$ W/cm^2, the $\tau_{rise} = 420$ ps produced less than 16 harmonics efficiently, while the $\tau_{rise} = 125$ ps produced more than 44 harmonics efficiently.

Both the Imacon streak camera data and the study involving changes in the laser risetime tend to support the arguments that transient density profile effects must be included if we are to understand these nonlinear phenomena.

Conclusions

The existence of very steep density profiles and high upper shelf densities imply that the CO_2 laser deposits its energy spatially quite close to the ablation surface where calculations indicate that a high degree of symmetry must exist in order to achieve the necessary high compression ratios. Thus, energy transport provides only limited

improvement in the ablative symmetry over that achieved in the irradiation symmetry. Current data suggests that a balance between radiation pressure and hydrodynamic pressure underestimates the density to which the CO_2 laser light penetrates for early times. However, the balance condition indicates that in Helios laser operational conditions, the bulk of the deposited laser energy through the resonance absorption process is deposited at densities at or above 10^{21} e/cm^3, the Nd:glass critical density. This implies that symmetrization through transport should be similar for CO_2 and Nd:glass, if we ignore hot electrons. However, all data for CO_2 is consistent with all of the absorbed laser energy first being deposited into hot electrons. Since the hot electron temperature scales in PIC numerical simulations,[19] like

$$T_{hot} \sim (I\lambda^2 T_e)^{1/3}, \qquad (1?)$$

any process which locally increases the laser intensity will cause T_{hot} to rise. Further, if a portion of the beam self-focuses, while the remainder of the laser light focuses linearly, we would expect both a super-hot and a hot electron distribution to result. Both particle diagnostics, namely electron spectrometers[20] and Thomson parabolas,[21] as well as hard x-ray diagnostics[22] are indicating a T_{hot}, possibly as high as 400 keV at $1 - 3 \times 10^{16}$ W/cm^2. While current data is not capable of distinguishing between a one or two hot-electron temperature distribution, a plausible explanation is that two distributions exist and self-focusing could be a contributing effect. The existence of laser filamentation, if established, opens up the possibilities for other

instabilities, like, for example, stimulated Raman scattering. This particular instability also can cause super-hot electrons to be produced. To date, direct inferences of stimulated Raman scattering through the preliminary observations of either half harmonic or high half-integer harmonic light indicate that it can occur, but only under special circumstances and then only at very low conversion efficiencies.

Much more work and understanding is required on all of these instabilities because of their intimate connection to the energy distribution functions for both the particles and the x rays. Since the effective ranges for both particles and x rays are energy dependent, the effect on both symmetry and preheat of the transported energy by these carriers can be assessed only if correct distribution functions and scaling laws are included in the calculations. Thus, studies which lead to an understanding and characterization of these distribution functions are essential. In particular, the fact that radiation pressure balance underestimates the density to which the CO_2 radiation penetrates, while the time scale for the balance condition to apply has been unknown, present calculations tend to cause too few particles to be overheated at early times. Further work on the visible harmonics should be able to provide all the necessary information required to correctly model this early-time portion of the problem. Since preheat is most damaging at early times, correct modeling here is very important.

The author wishes to thank R. Godwin, C. Grantill and P. Forslund for several helpful discussions, as well as the Helios and Gemini operations crews, the target fabrication team, N. Clabo, D. van Hulsteyn and F. Wittman for their help in obtaining the data.

References

1. R. L. Carman, D. W. Forslund and J. M. Kindel, Phys. Rev. Lett. 46, 29 (1981).
2. D. T. Attwood, D. W. Sweeney, J. M. Auerbach and P.H.Y. Lee, Phys. Rev. Lett. 40, 184 (1978).
3. D. W. Forslund, J. M. Kindel, K. Lee, E. L. Lindman and R. L. Morse, Phys. Rev. A11, 679 (1975); K. Lee, D. W. Forslund, J. M. Kindel and E. L. Lindman, Phys. Fluids 20, 51 (1977); K. G. Estabrook, E. J. Valeo and W. L. Kruer, Phys. Fluids 18, 733 (1975); G. Auer, K. Sauer, K. Baumgartel, Phys. Rev. Lett. 42, 1744 (1979).
4. E. A. McLean, J. A. Stamper, B. H. Ripin, H. R. Griem, J. M. McMahon and S. E. Bodner, Appl. Phys. Lett. 31, 825 (1977).
5. N. H. Burnett, H. A. Baldis, M. C. Richardson and G. D. Enright, Appl. Phys. Lett. 31, 172 (1977).
6. R. L. Carman, C. K. Rhodes and R. F. Benjamin, submitted for publication.
7. M. J. Herbst, J. A. Stamper, R. R. Whitlock, R. H. Lehmberg and B. H. Ripin, Phys. Rev. Lett. 46, 328 (1981).
8. H. A. Baldis and P. B. Corkum, Phys. Rev. Lett. 45, 1760 (1980).
9. P. L. Kelley, Phys. Rev. Lett. 1' 1005 (1965).
10. D. V. Giovanielli, J. E. Kephart and A. H. Williams, J. Appl. Phys. 47, 2907 (1976).
11. Work performed by J. E. Kephart of the Los Alamos National Laboratory.
12. J. Reintjes, R. L. Carman and T. Shimizu, Phys. Rev. A8, 1486 (1973); M. M. T. Loy and Y. R. Shen, Phys. Rev. Lett. 25, 1333 (1970); J. A. Fleck, Jr. and R. L. Carman, Appl. Phys. Lett. 20, 290 (1972).

13. R. L. Carman, J. Hanus and D. L. Weinberg, Appl. Phys. Lett. 11, 250 (1967).

14. R. L. Carman, R. Y. Chiao and P. L. Kelley, Phys. Rev. Lett. 17, 1281 (1966).

15. F. Shimizu, Phys. Rev. Lett. 19, 1097 (1967).

16. R. H. Lehmberg, Phys. Rev. Lett. 41, 863 (1978).

17. Work performed by R. F. Benjamin of the Los Alamos National Laboratory.

18. Work performed by J. McLeod of the Los Alamos National Laboratory.

19. D. W. Forslund, J. M. Kindel and K. Lee, Phys. Rev. Lett. 39, 284 (1977); K. Estabrook and W. L. Kruer, Phys. Rev. Lett. 40, 42 (1978).

20. T. H. Tan, G. H. McCall and A. H. Williams, Los Alamos National Laboratory Report, LA-UR-80-900 (1980).

21. F. Begay, Bull. Am. Phys. Soc. 25, 1010 (1980).

22. W. Priedhorsky, D. Lier, R. Day and D. Gerke, Bull. Am. Phys. Soc. 25, 885 (1980).

TABLE I

The self-focusing lengths calculated for $P_{critical} = 10^8$ W and d = 50 μm and 100 μm.

I (W/cm^2)	Z_{SF}(50 μm)	Z_{SF} (100 μm)
10^{12}	436 μm	872 μm
10^{13}	138 μm	276 μm
10^{14}	49 μm	98 μm
10^{15}	14 μm	28 μm

Figure Captions

Fig. 1. Compilation of data previously published in Ref. 4 and 5. Presented is the relative harmonic conversion efficiency in the backscatter direction normalized to laser light backscattered plotted versus harmonic number. The parameter $I\lambda^2$ has been held constant at $I\lambda^2 \sim 10^{16}$ W $\mu m^2/cm^2$. Note the similar behavior for both the 1 μm and 10 μm irradiation.

Fig. 2. Visible harmonic spectra obtained in CO_2 laser fusion experiments at the Gemini and Helios laser facilities: (a) Gemini data for plane $(CH_2)_x$ target at $I_L \sim 5 \times 10^{14}$ W/cm^2 showing the 16th through 20th harmonics produced at the same conversion efficiency, (b) Helio. data for spherical $(CH_2)_x$ coated BeCu target at $I_L \sim 3 \times 10^{16}$ W/cm^2 showing the 16th through 27th harmonics obtained in second order, as well as the 25th through 29th harmonics obtained in the third order spectrum (weaker satellites in the left-hand portion of the spectrum).

Fig. 3. X-ray pinhole camera photographs taken simultaneously by a 25- and 50-μm-diam pinhole doublet. The two pinholes are separated by ~ 1 mm. The x-ray filtering leads to a peak sensitivity at ~ 1 keV. The four sets of photographs were taken using carbon-wire targets under otherwise identical conditions, except (a) $I \sim 10^{14}$ W/cm^2 (b) $I \sim 1.4 \times 10^{15}$ W/cm^2, (c) $I \sim 4.3 \times 10^{15}$ W/cm^2, and (d) $I \sim 2.3 \times 10^{15}$ W/cm^2. The direction of elongation is parallel to the target cylindrical axis indicating electron transport towards the target holder. The resolution-limited x-ray sources are consistent with self-focusing of the incident CO_2 radiation, but the extended size of the x-ray image along the target axis also suggests that return-current pinching could be occurring.

Fig. 4. High resolution spectrum of 16th harmonic obtained with a 1.0-m McPherson spectrograph at the Helios laser facility operated at 600 J/beam. Note the two distinct frequency modulations in the spectrum.

Fig. 5 Spectra of self-focused filament light created by a Nd:glass ps laser. The photographs were obtained by imaging the end of a 6 cm cell containing various liquids onto the slit of a Spex 0.75-m spectrograph with a magnification of 10:1. The liquids were (a) CS_2 (b) toluene, (c) benzene, (d) nitrobenzene, and (e) Hg calibration lamp. These spectra were taken from J. Reintjes, etal. (Ref. 12).

Fig. 6. Sketch of the qualitative effect on the density profile expected at peak laser irradiance as the laser pulse risetime is changed from very short τ_1 to quite long τ_3. The parameter δ is meant to set an approximate spatial scale and is the laser skin depth.

Fig. 7. Retraces of eight oscillograms taken with the Los Alamos Model 76 oscilloscope (5.0 GHz bandwidth) and a Moletron P-500 pyroelectric detector which looked at a beamsplit portion of the incident laser light. One class of pulse shapes and intensities produced no high harmonics while the other class produced copious quantities of high harmonics.

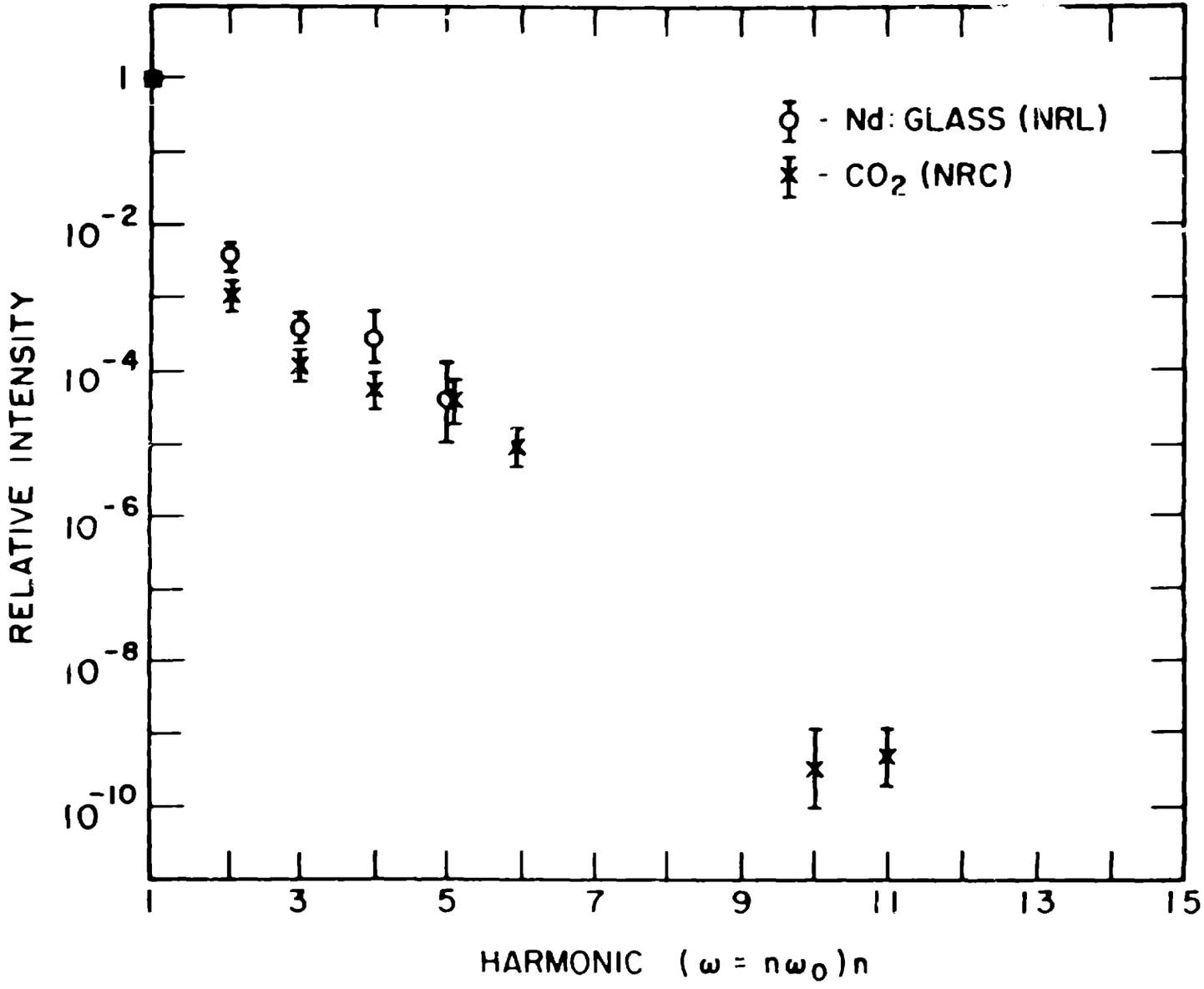
RELATIVE INTENSITY
1
10^{-2}
10^{-4}
10^{-6}
10^{-8}
10^{-10}
1
3
5
7
9
11
13
15
HARMONIC ($\omega = n\omega_0$)n
- Nd: GLASS (NRL)
- CO_2 (NRC)

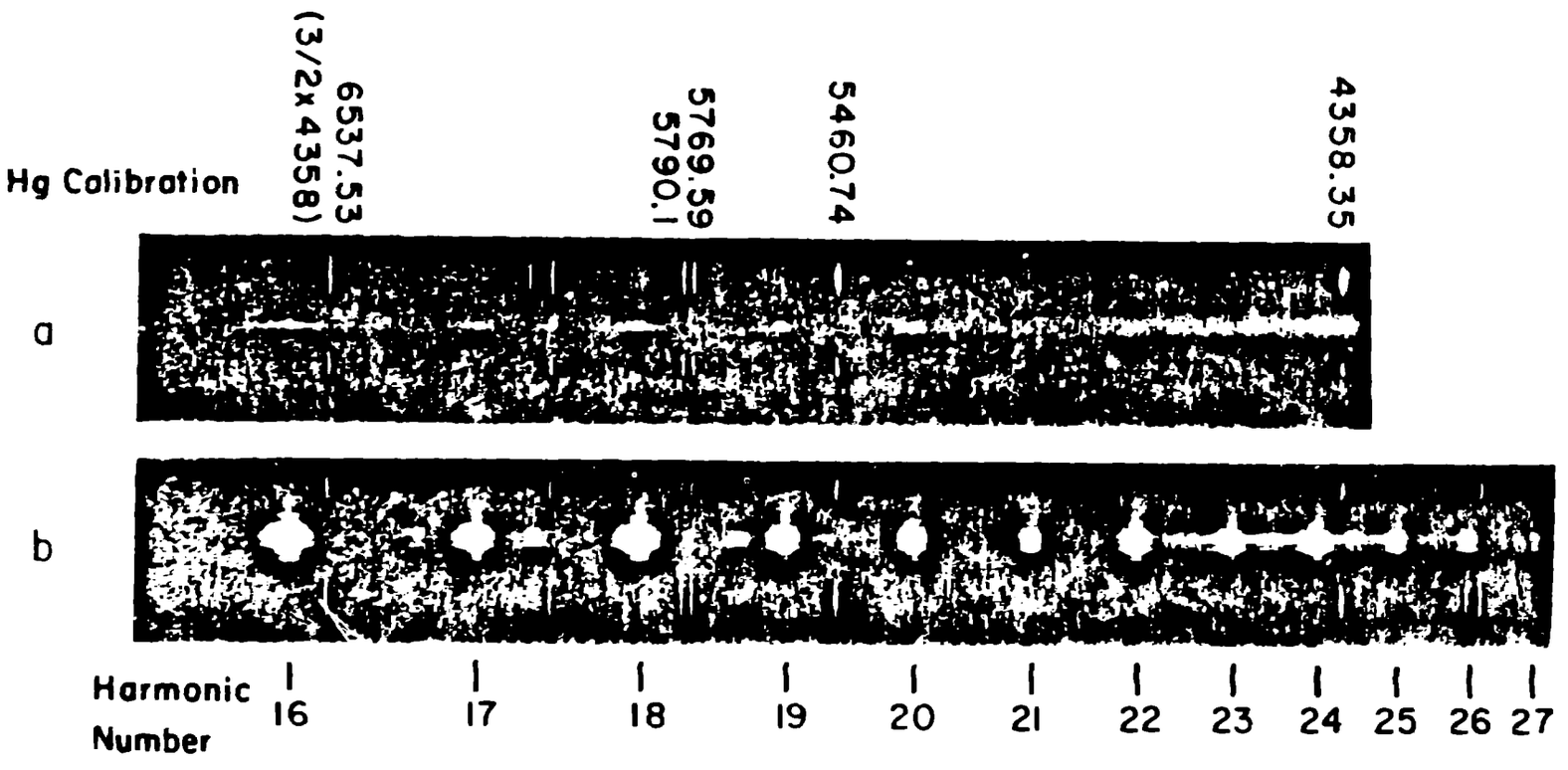
Hg Calibration
6537.53 (3/2x4358)
5769.59
5790.1
5460.74
4358.35
a
b
Harmonic Number
16
17
18
19
20
21
22
23
24
25
26
27

a

b

c

d

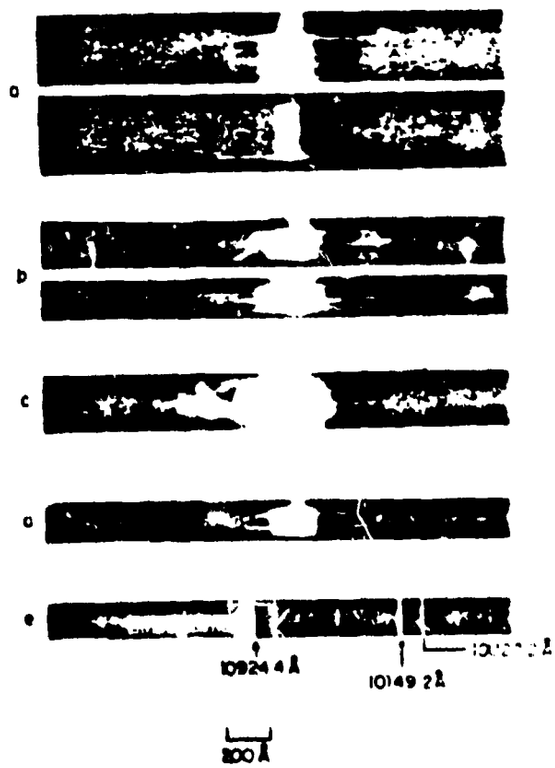
a
b
c
d
e
10924 4 Å
10149 2 Å
200 Å

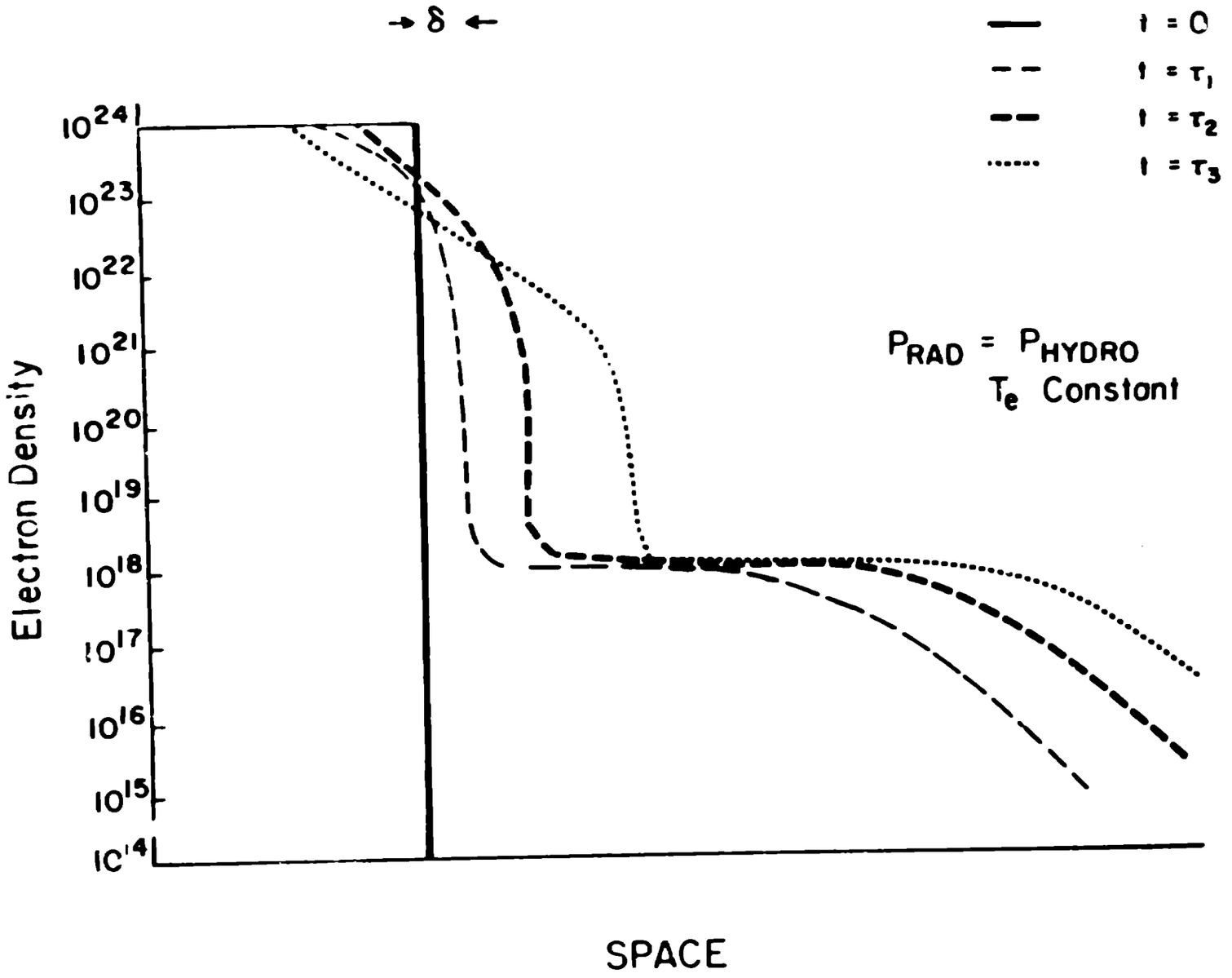
→ δ ←
t = 0
t = τ1
t = τ2
t = τ3
Electron Density
10^24
10^23
10^22
10^21
10^20
10^19
10^18
10^17
10^16
10^15
10^14
P_RAD = P_HYDRO
T_e Constant
SPACE

Shot 21042008
520 ps Risetime
1750 ps FWHM
E=245 J
$I=2.4 \times 10^{14}$ w/cm^2

Shot 21042105
230 ps Risetime
900 ps FWHM
E=176 J
$I=4 \times 10^{14}$ w/cm^2

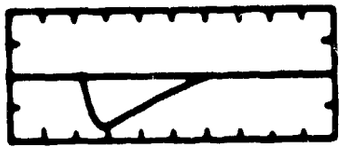

Shot 21042204
230 ps Risetime
900 ps FWHM
E=269 J
Double Pulse

Shot 21042308
420 ps Risetime
1700 ps FWHM
E=330 J
$I=2.2 \times 10^{15}$ w/cm^2

NO HIGH HARMONICS PRODUCED

Shot 20093003
125 ps Risetime
700 ps FWHM
E=285 J
$I=2.5 \times 10^{15}$ w/cm^2

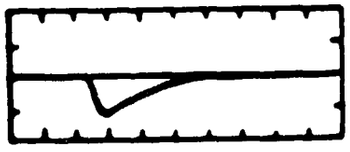

Shot 20100103
160 ps Risetime
650 ps FWHM
E=154 J
$I=4.9 \times 10^{15}$ w/cm

Shot 20100702
175 ps Risetime
800 ps FWHM
E=174 J
$I=3.8 \times 10^{15}$

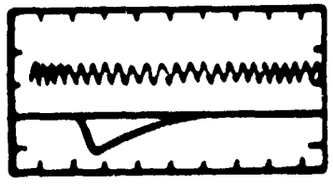

Shot 20100904
140 ps Risetime
800 ps FWHM
E=154 J
$I=2.3 \times 10^{15}$ w/cm^2

COPIOUS HIGH HARMONICS PRODUCED